Moisture-triggered ambient-temperature carbonatization of main group II metal oxides under elevated CO_2 pressure

Georg Gravogl[1,2], Christian Knoll,[2,3] Werner Artner,[4] Elisabeth Eitenberger,[5] Gernot Friedbacher,[5] Andreas Werner,[6] Michael Harasek,[3] Peter Weinberger,[2] Danny Müller,[2]* Ronald Miletich[1]

[1] Institut für Mineralogie und Kristallographie, University of Vienna, Althanstraße 14, 1090 Vienna, Austria

[2] Institute of Applied Synthetic Chemistry, TU Wien, Getreidemarkt 9/163-AC, 1060 Vienna, Austria

[3] Institute of Chemical, Environmental & Biological Engineering, TU Wien, Getreidemarkt 9, 1060 Vienna, Austria

[4] X-Ray Center, TU Wien, Getreidemarkt 9, 1060 Vienna, Austria

[5] Institute of Chemical Technologies and Analytics, TU Wien, Getreidemarkt 9/164, 1060 Vienna, Austria

[6] Institute for Energy Systems and Thermodynamics, TU Wien, Getreidemarkt 9/302, 1060 Vienna, Austria

danny.mueller@tuwien.ac.at

Abstract

The reversible reaction of metal oxides with CO_2 forming metal carbonates with concomitant release of energy is considered as a promising concept for thermochemical energy storage. One major advantage of thermochemical energy storage materials is the possibility of a lossless mid-term and long-term storage of waste heat. Metal carbonates provide high-energy densities and were so far investigated for their application in high-temperature processes. Inspired by the carbonatization of (main group II) metal oxides in nature during mineralization and CO_2 fixation in the presence of moisture under elevated pressures, the Me (II) oxides (Me = Mg, Ca, Sr, Ba) were investigated with respect to their reactivities with CO_2 at pressures up to 55 bar and ambient temperature. Whereas for MgO none of the applied conditions yielded any formation of a carbonate phase, the other oxides revealed appropriate reactivities by forming corresponding carbonates under considerably mild reaction conditions.

Keywords: main group II oxides, main group II carbonates, low-temperature carbonatization, in-situ powder X-Ray diffraction, thermochemical energy storage

1. Introduction

Reliable energy supply has become a fundamental in today's society. Although notable efforts were made within the last decade to decrease the ecological footprint of the global energy supply by supporting sustainable energy sources, fossil raw materials are still the fundamental resource for energy production. (Shine, 2005) Aiming for an increased awareness of sustainable energy management the International Energy Agency (IEA) reported in 2011, that the global energy loss in form of waste heat during electricity generation accounts for approximately 66 %. (IEA, 2011) This stimulated equally politics and science to focus on a reduction and recycling of waste heat to contribute to a more efficient energy management. (IEA, 2014; Arce et al., 2011)

A major challenge for waste heat management is the temporal mismatch between heat production and consumption. (Solé et al., 2012) Therefore, a feasible approach towards a more efficient energy balance could be the storage of so far unused waste heat, allowing for a decoupling of production and consumption in space and

Selection and/or peer review under responsibility of Scientific Committee
doi:10.18086/swc.2017.14.01 Available at http://proceedings.ises.org

time. (Zhang et al., 2016) The concept of thermal energy storage enables the transfer of excess energy to a suitable storage medium, thus preserving the stored energy for the case of a sudden demand. (Bauer et al., 2012; Abedin, 2011) Several methods categorized according to the used storage medium, are known for this purpose. Whereas sensible (Dinker et al., 2015) and latent heat storage (Zalba et al., 2003) transferring the heat to a liquid or solid storage medium, respectively to a phase-change material are mainly suitable for low- to medium-temperature storage, thermochemical energy storage (TCES) offers a much larger temperature compatibility, being tunable by the applied storage reaction. (Abedin, 2011; Cot-Gores et al., 2012) By charging the storage material (*A*, Eq.1) with the waste heat its dissociation is forced, liberating a reactive gas (*B*, Eq.1) as H_2O, CO_2, O_2, NH_3, … Once the formed decomposition product (*C*, Eq. 1) is contacted with the reactive gas under suitable reaction conditions, the back-reaction takes place, discharging the stored energy. A general equation for a thermochemical energy storage reaction is given in Eq.1.

$$A + \Delta H \leftrightharpoons B + C \tag{1}$$

Compared to sensible and latent heat storage, thermochemical storage offers - besides the broad applicable temperature range (between room-temperature and 1200 °C in *e.g.* concentrating solar power plants (Prieto et al., 2016)) - notably higher energy densities, decreasing amounts of necessary material. Moreover, it avoids insulation of the material once charged, as until contacted with the reactant no discharging will occur. The possibility of lossless storage lends TCES-materials for mid-term to long-term storage applications, (Xu, 2014) where *e.g.* waste heat is continuously stored but liberated periodically to fit heat-demands going beyond the daily process routine. For such applications a storage at preferably room-temperature would be desirable, followed by a discharging of the material at low-temperatures avoiding a preheating of the material.

A class of TCES-materials featuring relatively high energy contents are metal carbonates, (Kyaw et al., 1996; Yamauchi et al., 2007) commonly investigated for application at elevated temperatures in combination with *e.g.* concentrating solar power plants. (Reich, 2014; Rhodes et al., 2015) Recently we could demonstrate, that various metal oxides (obtained from decomposition of the corresponding carbonates) undergo carbonatization already at moderate temperatures in the presence of moisture and by increasing the partial pressure of CO_2 to 55 bar. (Müller et al., 2017a)

Main-group II metal oxides were so far mainly known as TCES-materials with respect of being considered for hydrate reactions. In order to broaden the scope of applicability, the process of CO_2 sequestration in rock mineralization (Fagerlund et al., 2012; Sissmann et al., 2014; Yamauchi et al., 2007; Morales-Flórez et al., 2015) inspired this endeavour reported here. Carbonatization reactivity at low-temperatures and elevated CO_2 pressures were studied aiming for novel low-temperature carbonate TCES-materials for mid- and long-term storage.

2. Results and Discussion

2.1 Carbonatization of MgO

Among the different main-group II metal oxides in particular MgO appears to be perfectly suitable for an application in thermochemical energy storage due to its availability as industrial raw material. It is known from earlier studies on the hydration behavior of MgO, which also have been aiming for a TCES-process, that the calcination conditions determine the reactivity of the material. Previous work on $Mg(OH)_2$-calcination resulted in calcination conditions providing a notably reactive material (Müller et al., 2017b), which was also used in the current low-temperature carbonatization study.

Successful carbonatization of MgO was already reported for reactions at temperatures around 575 °C (Fagerlund et al., 2012). Nevertheless, at ambient temperatures under the applied conditions varying from 8 bar wet CO_2 in the *in-situ* P-XRD setup (see experimental) to 55 bar wet CO_2 in the autoclave, in none of the experiments terminated after 2 h any detectable trace of $MgCO_3$ has been found. The same negative result accounts for experiments at temperatures up to 60 °C in the autoclave. The most likely explanation for the absence of any reactivity is the relatively high energetic barrier of the CO_2-absorption, which cannot be overcome by simply

increasing the CO_2-pressure. In order to investigate even higher CO_2-pressures under supercritical conditions, MgO was exposed to H_2O and kept for 4 h in a supercritical CO_2-reactor at 150 °C, 150 bar. In this case a complete conversion to $Mg(OH)_2$ can be observed, but still no reaction with CO_2 and hence no carbonate formation occurs.

A notable kinetic hindrance was already reported in literature (Hu et al., 2011) not only for the CO_2-absorption on the MgO surface, but also for the H_2O dissociation on a MgO surface forming $Mg(OH)_2$. To exclude, that the carbonatization of MgO is hampered by a required intermediate formation of $Mg(OH)_2$, all experiments were repeated using $Mg(OH)_2$ as a precursor material. Nevertheless, even the choice of reactant material reveals to be not critical for the observed absence of any significant carbonatization.

Most recently it was shown, that the energetic barrier of the H_2O-dissociation on the MgO surface could be notably decreased by the dotation of the MgO lattice with a degree of dotation by up to 10 % of Ca^{2+}-ions (Müller et al., 2017c). In order to derive, whether a similar effect could also be observed in the case of the carbonatization, samples of $Mg_{1-x}Ca_xO$ with Ca-contents x = 0-1 were moistened and kept for 2 h at 55 bar in the autoclave. The phase composition of the different samples after 2 h reaction time is shown in Figure 1.

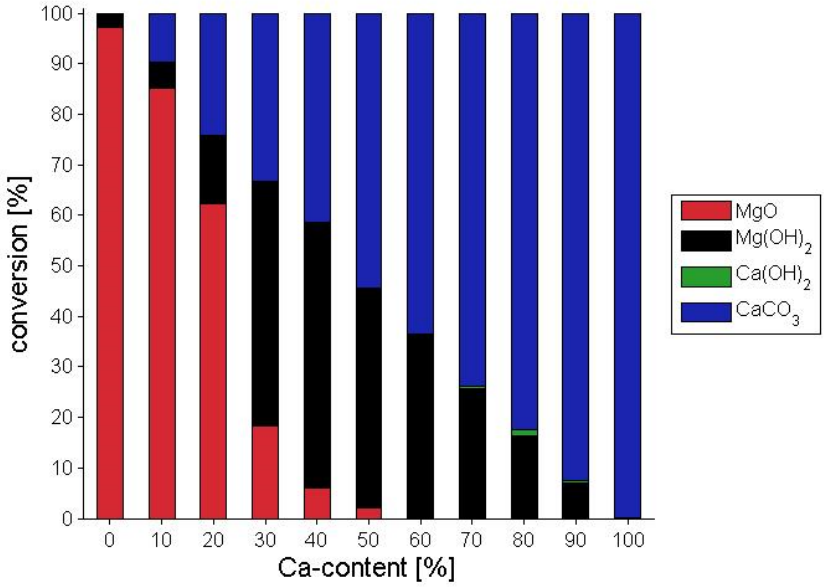

Fig. 1: Phase composition after 2 h reaction time of the $Mg_{1-x}Ca_xO$ samples in the presence of moisture at 55 bar CO_2

Phase analyses as carried out by means of X-ray powder diffraction gave evidence for significant conversion to carbonate for the Ca^{2+}-doped MgO materials, with a selective carbonate formation on the Ca^{2+}-components. Starting from the sample with 10 % Ca^{2+}-dotation, the complete amount of Ca^{2+}-dopant was carbonated, whereas the MgO component remained unchanged, or was partially hydrated forming $Mg(OH)_2$. The same result was obtained, when the mixed hydroxides $Mg_{1-x}Ca_x(OH)_2$ were used as starting material for carbonatization (see figure 2).*

* The phase composition of a comparable experiment regarding the reactivity of both the mixed oxides $Mg_{1-x}Ca_xO$ and hydroxides $Mg_{1-x}Ca_x(OH)_2$ in the absence of moisture are shown in Figure S1 and S2.

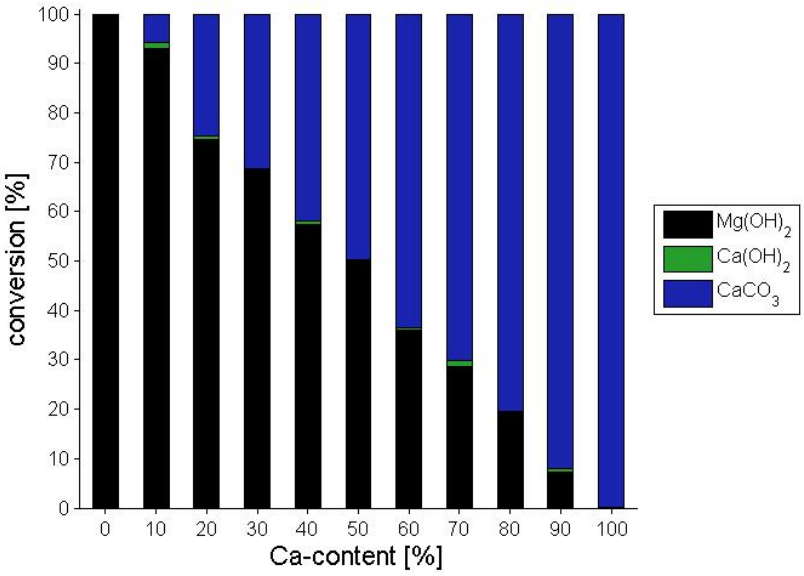

Fig. 2: Phase composition after 2 h reaction time of the $Mg_{1-x}Ca_x(OH)_2$ samples in the presence of moisture at 55 bar CO_2

This allows for the conclusion, that although a Ca^{2+}-dotation can effectively promote the H_2O dissociation, no similar catalytic effect is found in the case of the CO_2-absorption.

2.2 Carbonatization of CaO

Based on the promising carbonatization results of the Ca^{2+}-doped MgO samples, and demonstrating the favorable transformation of the CaO components to the corresponding carbonate within 2 h at 55 bar and room-temperature, as a result both the time dependency of the reaction and the influence of the moisture concentration has been investigated.†

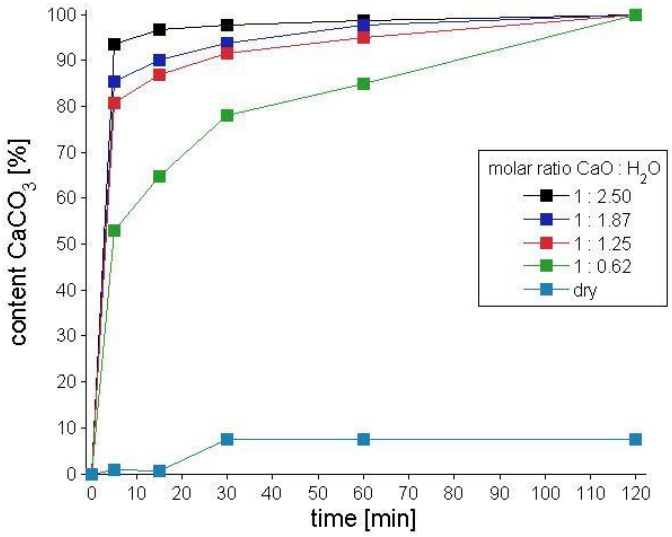

Fig. 3: Time- and moisture dependent carbonatization of CaO at 55 bar CO_2

Figure 3 shows the time dependent increase of the $CaCO_3$-concetration for 5 different moisture concentrations, ranging between 0 and 2.5 molar equivalents of H_2O per equivalent CaO. Without additional moisture, the initial

† Prior experiments on CaO-carbonatization in the P-XRD at 8 bar of wet CO_2 resulted only incomplete conversion to 34 % $CaCO_3$ after 120 minutes. (Müller et al., 2017a)

CaO is converted to 9 % into $CaCO_3$, keeping this phase composition constant over the observed time. Already after 5 minutes, more than 50 % of CaO are carbonated for the various amounts of added H_2O. In the case of 2.5 equivalents of H_2O even 94 % $CaCO_3$ had formed. The CaO phase was completely carbonated after 120 minutes for all investigated variations of H_2O contents. As even in the case of molar deficits of H_2O the complete carbonatization of CaO to $CaCO_3$ takes place, it indicates that H_2O appears to have only a catalytic role in the process, otherwise no quantitative $CaCO_3$ formation would have been possible. According to the SEM-images shown in figure S3 an increasing amount of H_2O present during the carbonatization promotes the observable fragmentation of the particles, facilitating easier access of reactive gas CO_2 to the remaining CaO.

Once a fully reversible reaction, which is potentially suitable for a TCES-process, has been identified another intriguing aspect is the cycle stability of the process. To assess the reproducibility of the quantitative CaO-carbonatization, the same sample of $CaCO_3$ was calcined at 900 °C for 1 h and re-carbonated in the autoclave at 55 bar in the presence of 0.62 equivalents H_2O for 120 minutes in 7 subsequent cycles. The phase composition of a representative sample after each cycle is shown in Figure 4.

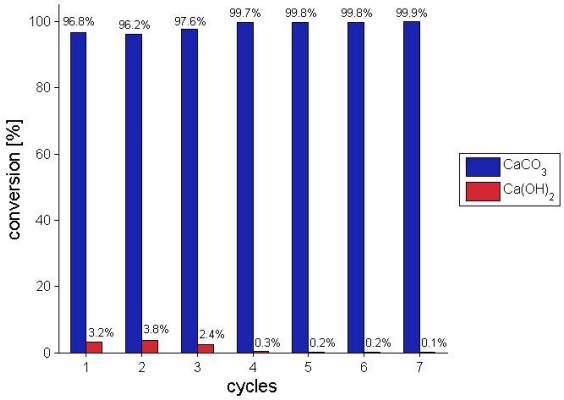

Fig. 4: Phase composition during cycle-stability test of $CaCO_3$ / CaO

For all 7 cycles after 120 minutes the carbonatization was found nearly quantitative, only in the first 3 cycles a small residue of <4 % $Ca(OH)_2$ could be observed. The reduction of the residual CaO is attributed to an increasing degree of particle fragmentation with the number of cycles, which in turn decreases the diffusion pathways for any volatile component. In the SEM-images in Figure 5, a fragmentation of the particles on repeated carbonatization / calcination process could be observed. In Figure 5a – showing CaO after the first calcination – a rather uniform particle size distribution is found. With increasing number of cycles also a fraction of smaller particles is observed, which results from the mechanical stress originating from the volume work accompanying the transformation from CaO to $CaCO_3$.

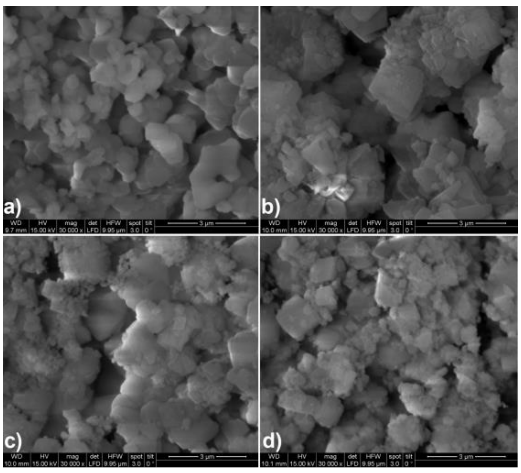

Fig. 5: SEM images of various stages of the cycle stability test a) CaO after first decomposition of $CaCO_3$ b) $CaCO_3$ after 1 cycle c) $CaCO_3$ after 4 cycles d) $CaCO_3$ after 7 cycles. Image size 9 x 9 µm

As the reaction $CaCO_3 \leftrightarrow CaO + CO_2$ revealed an attractive reactivity and cycle stability, subsequent investigations will focus on determination of the thermochemical parameters and energy density under the applied low-temperature carbonatization conditions.

2.3 Carbonatization of SrO

A direct comparison of the carbonatization behavior of MgO and CaO suggests an increased CO_2-affinity moving towards the heavier alkaline earth cations, correlating with the increased ionic radii. Attempted carbonation of SrO in the absence of H_2O failed both under 8 bar and 55 bar of CO_2, which could be anticipated based on the prior experience. In contrast, P-XRD patterns of the sample in the presence of moisture under 8 bar CO_2 reveal an interesting behavior as shown in Figure 6.

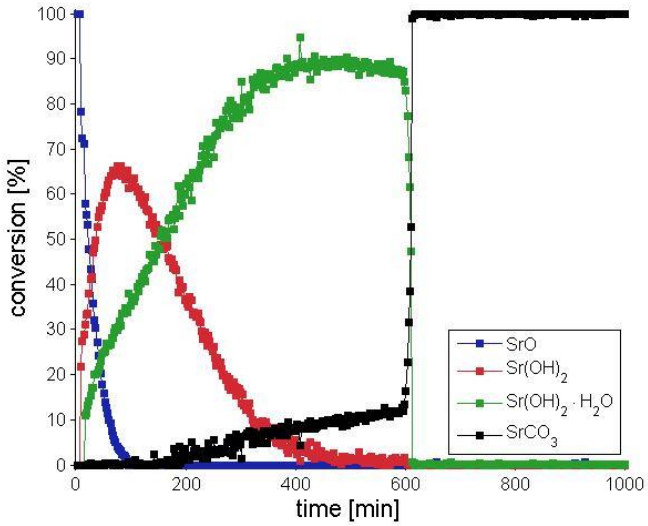

Fig. 6: Time-dependent phase composition of SrO during carbonatization in the presence of moisture at 8 bar CO_2

SrO is very hygroscopic, transforming immediately in the presence of H_2O to crystalline $Sr(OH)_2$ (red symbols). It directly hydrates yielding the monohydrate phase $Sr(OH)_2 \cdot H_2O$ (green symbols). This hydration process occurs simultaneously, and after 500 minutes the intermediate $Sr(OH)_2$ completely converted to $Sr(OH)_2 \cdot H_2O$. In parallel to this process after approximately 180 minutes the carbonatization starts at a nearly exact 1:1 ratio of $Sr(OH)_2$ to $Sr(OH)_2 \cdot H_2O$. The XRD pattern provides evidence for the formation of $SrCO_3$ as new phase (black symbols). Within the next 400 minutes the $SrCO_3$ phase augments slightly up to about 12 %, when suddenly the carbonatization gets significantly accelerated and the conversion is completed within a short time interval (*i.e.* 15 minutes). This spontaneous acceleration of the carbonatization rate was found to be reproducible on repeated experiments.

Apart of this unexpected carbonatization behavior, SrO behaves also different with respect to the role of H_2O in the process. Whereas in the case of CaO H_2O seems to have only a catalytic impact – under-stoichiometric H_2O amounts still allow for quantitative carbonatization of CaO, – in the case of SrO the intermediate $Sr(OH)_2 \cdot H_2O$ is the apparently critical reactive species. Once enough $Sr(OH)_2 \cdot H_2O$ had formed, the carbonatization starts from the surface of the particles, most likely forming a thin layer of $SrCO_3$ on the particle surface. As this $SrCO_3$ layer is denser than the original hydroxide phase, it acts as a barrier for diffusion of water and CO_2 into the inner bulk of the particles. A likely explanation for the observed sudden acceleration of the carbonatization rate is the formation of micro-cracks, mechanical changes including fragmentation of the particles as caused by the volume work and strain occurring at the interface between the hydrous phase and the carbonate.‡ Table S1 provides the corresponding crystallographic cell-parameters for SrO, $Sr(OH)_2$, $Sr(OH)_2 \cdot H_2O$ and $SrCO_3$. This interpretation is supported by SEM-images of SrO material before and after carbonatization (figure 7), as the images reveal a

‡ The carbonation of $Sr(OH)_2 \cdot H_2O$ to $SrCO_3$ goes along with an expansion of the cell about 68 %.

notable particle fragmentation during the carbonatization process.

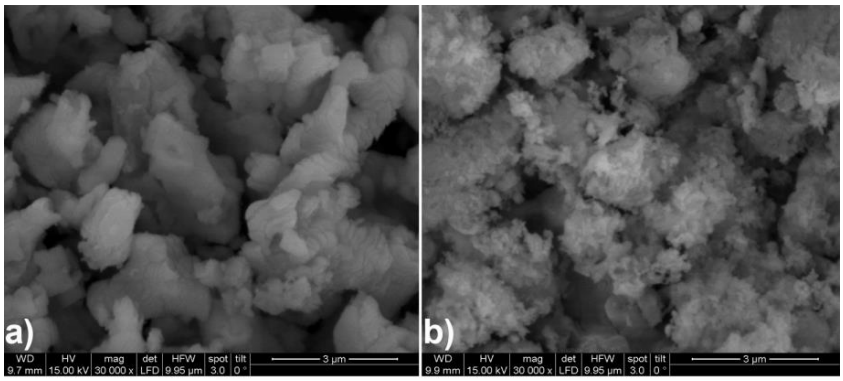

Fig. 7: SEM-images of a) SrO before carbonatization and b) $SrCO_3$ after carbonatization. Image size 9 x 9 µm

The same carbonatization experiment was repeated under 8 bar of wet CO_2, using a mixture of $Sr(OH)_2 \cdot 8H_2O$ (50 %) and $Sr(OH)_2 \cdot H_2O$ (50 %) as starting material in order to derive, whether a higher hydrate coordination around the Sr^{2+}-cation would significantly enhance the progress of the carbonatization process.

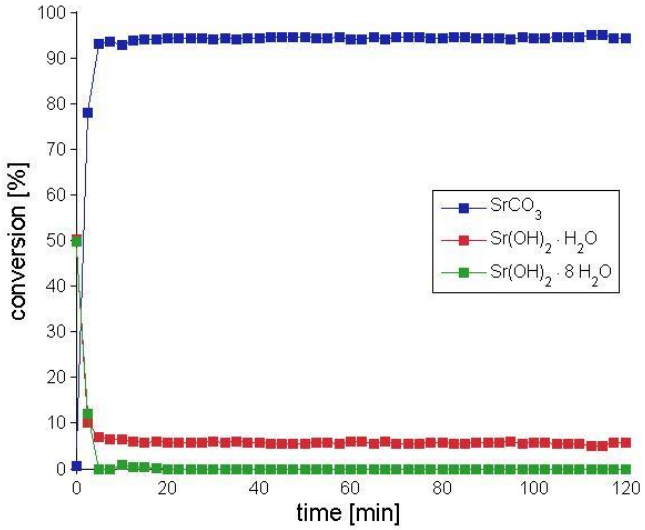

Fig. 8: Time-dependent phase composition of a mixture of $Sr(OH)_2 \cdot 8H_2O$ (50 %) and $Sr(OH)_2 \cdot H_2O$ (50 %) during carbonatization in the presence of moisture at 8 bar CO_2

Figure 8 reveals, that within 6 minutes the complete amount of $Sr(OH)_2 \cdot 8H_2O$ and 82 % of the $Sr(OH)_2 \cdot H_2O$ phase were converted into $SrCO_3$. The residual $Sr(OH)_2 \cdot H_2O$ was found inert towards further carbonatization within the next 120 minutes. This different carbonatization behavior allows for the conclusion, that carbonatization is favored by the higher hydrate coordination of Sr^{2+}.

2.4 Carbonatization of BaO

Based on the chemical similarity between Sr^{2+} and Ba^{2+} and the fact, that both form hydrated hydroxides, the behavior of BaO reacting with wet CO_2 was expected to be similar to that observed for SrO.

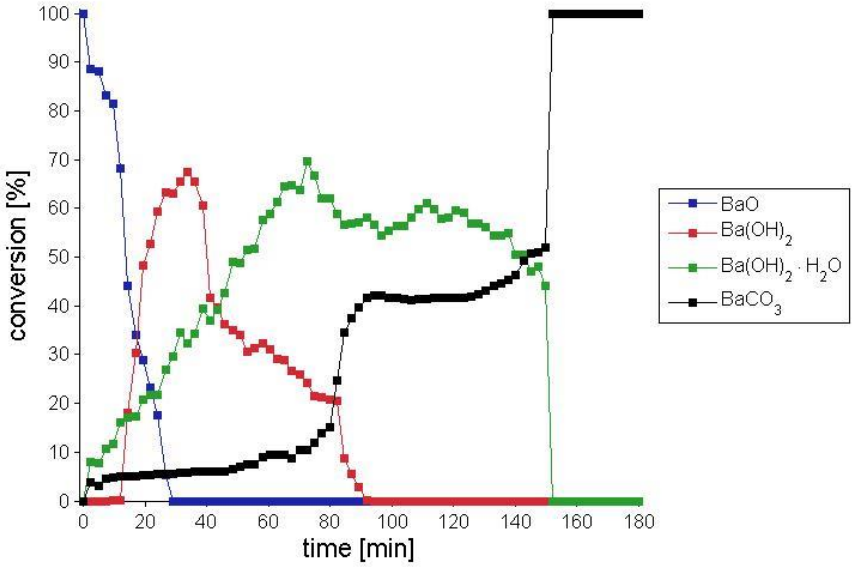

Fig. 9: Time-dependent phase composition of BaO during carbonatization in the presence of moisture under CO_2 atmosphere

Whereas in the case of SrO the carbonate formation initiated after formation of a 1:1 mixture between hydroxide and hydroxide monohydrate, in the case of BaO already after 2 minutes a small amount of the $BaCO_3$-phase is found. This may be attributed to a higher CO_2-affinity of Ba^{2+}, but also to the much faster conversion of BaO into the hydroxide and hydroxide monohydrate. In fact, the conversion of $Ba(OH)_2$ to $Ba(OH)_2{\cdot}H_2O$ is under the applied conditions so fast, that for the first 15 minutes only the $Ba(OH)_2{\cdot}H_2O$ – originating from the immediate hydration of the former $Ba(OH)_2$ – is observed. After that time also the $Ba(OH)_2$ phase increases, converting to the $Ba(OH)_2{\cdot}H_2O$ within 90 minutes. The carbonatization seems in the case of Ba^{2+} not as strictly related to the hydroxide monohydrate as in the case of Sr^{2+}. In fact, after the initial formation of around 5 % $BaCO_3$, the carbonate formation occurs via a two-step process with an intermediate plateau-phase: After 75 minutes the carbonatization rate increases, decelerating again once 42 % of $BaCO_3$ were formed. After 50 minutes of a nearly constant $BaCO_3$ content, only slightly increasing towards the end to 52 % $BaCO_3$, within 2 minutes a spontaneous completion yielding 100 % of $BaCO_3$ occurs. Based on the present data no final explanation of this in the series so far unique carbonatization process is possible.[§]

Also for Ba^{2+} a mixed sample of $Ba(OH)_2{\cdot}8H_2O$ (50 %) and $Ba(OH)_2{\cdot}H_2O$ (50 %) was compared regarding their carbonatization behavior (Figure 10).

[§] Table S2 provides the corresponding crystallographic cell-parameters for BaO, $Ba(OH)_2$, $Ba(OH)_2{\cdot}H_2O$ and $BaCO_3$.

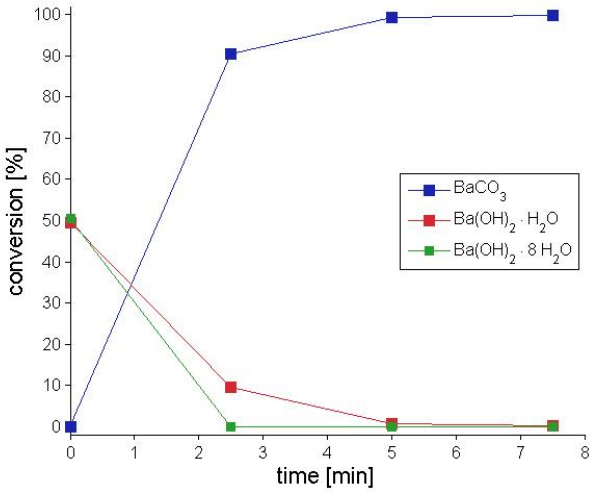

Fig.10: Time-dependent phase composition of a mixture of $Ba(OH)_2 \cdot 8H_2O$ (50 %) and $Ba(OH)_2 \cdot H_2O$ (50 %) during carbonatization in the presence of moisture at 8 bar CO_2

In the case of Ba^{2+} the carbonatization of both hydroxides is completed already within 5 minutes. Nevertheless, also in this case a slightly higher reactivity for the $Ba(OH)_2 \cdot 8H_2O$ is found, as after 2.5 minutes the complete octahydrate phase was carbonated, whereas still 12 % of $Ba(OH)_2 \cdot H_2O$ were present.

3. Conclusion

In the present study main group II oxides were investigated for their reactivity towards CO_2 in the presence of moisture at ambient temperature and elevated pressures up to 55 bar of CO_2. The aim of this approach was the investigation of a carbonatization process for main group II oxides regarding their application as long-term thermochemical storage materials with discharging of the stored energy near to ambient temperature.

From the investigated series of MgO, CaO, SrO and BaO, all oxides apart from MgO were found to carbonate under the applied conditions at the given time scales. The best performance was observed for CaO, transforming quantitatively to the corresponding carbonate in the presence of moisture at 55 bar CO_2 within 120 minutes. Repeated calcination / carbonatization of the material under the same conditions revealed a very appealing cycle stability of the process, although a concomitant particle fragmentation was observed, which can be attributed to the volume work involved into the reaction. In case of SrO the hydrate coordination sphere around the Sr^{2+} seems to have a notable impact on the calcination behavior. Treated with 8 bar wet CO_2, SrO was hydrated immediately to $Sr(OH)_2$ in a first step and consequently to $Sr(OH)_2 \cdot H_2O$, which was then the active phase reacting with CO_2 to form $SrCO_3$. An initial slow conversion rate observed for the carbonatization was suddenly accelerated and is assigned to particle changes, most likely due to the formation of micro-cracks and fragmentation. Additional experiments using $Sr(OH)_2 \cdot H_2O$ and $Sr(OH)_2 \cdot 8H_2O$ in carbonatization further supported the postulated importance of the hydrate coordination sphere around the cation, as in contrast to the monohydrate the octahydrate was quantitatively carbonated within 6 minutes. In the case of BaO a much higher carbonatization reactivity than for SrO, reaching complete conversion after 150 minutes, was found. Although, the reaction involves the intermediate formation of $Ba(OH)_2$ and $Ba(OH)_2 \cdot H_2O$, the carbonatization mechanism seems different, as a two-step carbonatization with an intermediate plateau was observed. Also in the case of Ba^{2+} the hydrate coordination sphere around the cation promotes the carbonatization.

Based on the present work regarding a general feasibility of an ambient-temperature carbonatization for main group II oxides, within a next step the thermochemical data and energy densities for the materials under the selected process parameters will be established. A further in-depth investigation of the impact of H_2O on a molecular level during the carbonatization process, as well as on the detailed carbonatization mechanisms for SrO and BaO is currently ongoing.

4. Experimental

4.1 Material

MgO (calcined from $Mg(OH)_2$,), CaO (calcined from commercially available $Ca(OH)_2$) and the mixed $Mg_{1-x}Ca_xO$ were prepared by thermal decomposition of the commercially available (or in the case of $Mg_{1-x}Ca_x(OH)_2$ freshly precipitated) hydroxides. All other materials were commercially obtained and used as supplied.

4.2 X-Ray Powder Diffraction

The powder X-ray diffraction measurements were carried out on a PANalytical X'Pert Pro diffractometer in Bragg-Brentano geometry using Cu $K_{\alpha1,2}$ radiation and an X'Celerator linear detector with a Ni-filter. For *in-situ* monitoring of experiments an Anton Paar XRK 900 reaction chamber was used. The sample was mounted on a hollow ceramic powder sample holder, allowing for complete perfusion of the sample with the reactive gas. The sample temperature is controlled directly via a NiCr-NiAl thermocouple and direct environmental heating. The diffractograms were evaluated using the PANalytical program suite HighScorePlus v4.6a. (Degen et al., 2014) A background correction and a $K_{\alpha2}$ strip were performed. Phase assignment is based on the ICDD-PDF4+ database ((http://www.icdd.com), the exact phase composition, shown in the conversion plots, was obtained via Rietveld-refinement incorporated in the program suite HighScorePlus v4.6a. (Degen et al., 2014) All phase quantifications based on P-XRD are accurate within ±5 %. For the carbonization experiments the pressure in the sample chamber was adjusted to 8 bar, maintaining a constant flow through the chamber of 0.4 L CO_2 min^{-1}. To investigate the carbonation in the presence of moisture, the CO_2 was passed through an external moisturiser. The CO_2 was bubbled through a 20 cm high water tank followed by a droplet-separator before contacting the sample in the reaction chamber. At the entrance of the reaction chamber the gas had a dew-point temperature of 23.2 °C with a constant sample temperature of 25 °C.

4.3 Carbonation in the reactor

For the carbonation of the metal oxides at higher CO_2 pressure a stainless-steel autoclave with a volume of 0.19 L was used. A small amount of the metal oxides (around 250 mg) was placed in a glass-vial with perforated cap to avoid cross-contamination during pressure release and moistened with 200 µL H_2O. The reactor was pressurized with CO_2 at 55 bar unless otherwise stated, controlling the internal pressure with the integrated manometer of the reactor. The carbonation process was stopped after the specified reaction time by releasing the CO_2.

4.4 Scanning Electron Microscopy

SEM images were recorded on gold coated samples with a Quanta 200 SEM instrument from FEI under low-vacuum at a water vapor pressure of 80 Pa to prevent electrostatic charging.

5. References

1. Keith Shine, J.F., Kinfe Hailemariam, Nicola Stuber, 2005. Alternatives to the Global Warming Potential for Comparing Climate Impacts of Emissions of Greenhouse Gases. climatic change 3, 281-302.
2. IEA, 2011. Co-generation and Renewables. Solutions for a low-carbon energy future. https://www.iea.org/publications/freepublications/publication/co-generation-and-renewables-solutions-for-a-low-carbon-energy-future.html
3. IEA, 2014. Heating without global warming: Market developments and policy considerations for renewable heat.
4. Arce, P., et al., 2011. Overview of thermal energy storage (TES) potential energy savings and climate change mitigation in Spain and Europe. Applied Energy 8, 2764-2774.
5. Solé, A., et al., 2012. Parameters to take into account when developing a new thermochemical energy storage system. Energy Procedia 380-387.
6. Zhang, H., et al., 2016. Thermal energy storage: Recent developments and practical aspects. Progress in Energy and Combustion Science 1-40.

7. Bauer, T., et al., 2012. Thermal Energy Storage Materials and Systems. Annual Review of Heat Transfer 15, 131-177.
8. Ali H. Abedin, M.A.R., 2011. A Critical Review of Thermochemical Energy Storage Systems. The Open Renewable Energy Journal 42-46.
9. Dinker, A., M. Agarwal, and G.D. Agarwal, 2015. Heat storage materials, geometry and applications: A review. Journal of the Energy Institute
10. Zalba, B., et al., 2003. Review on thermal energy storage with phase change: materials, heat transfer analysis and applications. Applied Thermal Engineering 3, 251-283.
11. Cot-Gores, J., A. Castell, and L.F. Cabeza, 2012. Thermochemical energy storage and conversion: A-state-of-the-art review of the experimental research under practical conditions. Renewable and Sustainable Energy Reviews 7, 5207-5224.
12. Prieto, C., et al., 2016. Review of technology: Thermochemical energy storage for concentrated solar power plants. Renewable and Sustainable Energy Reviews 909-929.
13. J. Xu, R.Z.W., Y. Li, 2014. A review of available technologies for seasonal thermal energy storage. Solar Energy 610-638.
14. Kyaw, K., H. Matsuda, and M. Hasatani, 1996. Applicability of Carbonation/Decarbonation Reactions to High-Tempereture Thermal Energy Storage and Temperature Upgrading. Journal of Chemical Engineering of Japan 1, 119-125.
15. Yamauchi, K., N. Murayama, and J. Shibata, 2007. Absorption and Release of Carbon Dioxide with Various Metal Oxides and Hydroxides. Materials Transactions 10, 2739-2742.
16. Reich, L., 2014. Towards Solar Thermochemical Carbon Dioxide Capture via Calcium Oxide Looping: A Review. Aerosol and Air Quality Research
17. Rhodes, N.R., et al., 2015. Solar Thermochemical Energy Storage Through Carbonation Cycles of $SrCO_3$/SrO Supported on $SrZrO_3$. ChemSusChem 22, 3793-3798.
18. Müller, D., et al., 2017a. Low-temperature carbonation of metal oxides. Journal of Materials Science, submitted.
19. Fagerlund, J., J. Highfield, and R. Zevenhoven, 2012. Kinetics studies on wet and dry gas–solid carbonation of MgO and $Mg(OH)_2$ for CO_2 sequestration. RSC Advances 27, 10380.
20. Sissmann, O., et al., 2014. Enhanced Olivine Carbonation within a Basalt as Compared to Single-Phase Experiments: Reevaluating the Potential of CO_2-Mineral Sequestration. Environmental science & technology 10, 5512-5519.
21. Morales-Flórez, V., et al., 2015. Hydration and carbonation reactions of calcium oxide by weathering: Kinetics and changes in the nanostructure. Chemical Engineering Journal 194-200.
22. Müller, D., et al., 2017b. An in-situ powder X-Ray diffraction study on the rehydration-reactivity of low temperature calcined $Mg(OH)_2$. Applied Energy, submitted.
23. Hu, X.L., et al., 2011. Trends in water monomer adsorption and dissociation on flat insulating surfaces. Physical Chemistry Chemical Physics 27, 12447.
24. Müller, D., et al., 2017c. Calcium Dotation Facilitates Water Dissociation in Magnesium Oxide. Advanced sustainable materials, submitted.
25. Degen, T., et al., 2014. The HighScore suite. Powder Diffraction S2, S13-S18.
26. http://www.icdd.com,

6. Appendix

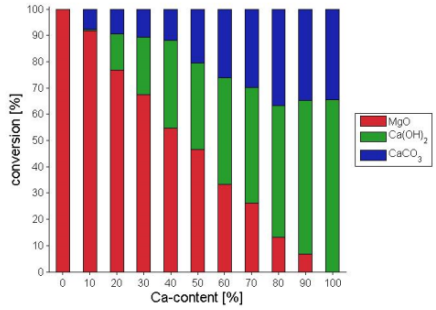

Fig. S1: Phase composition after reaction time of 2h of the $Mg_{1-x}Ca_xO$ samples in the absence of moisture at 55 bar CO_2

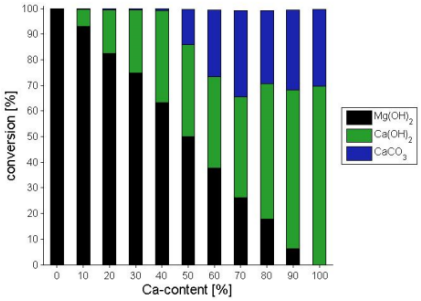

Fig. S2: Phase composition after reaction time of 2h of the $Mg_{1-x}Ca_x(OH)_2$ samples in the absence of moisture at 55 bar CO_2

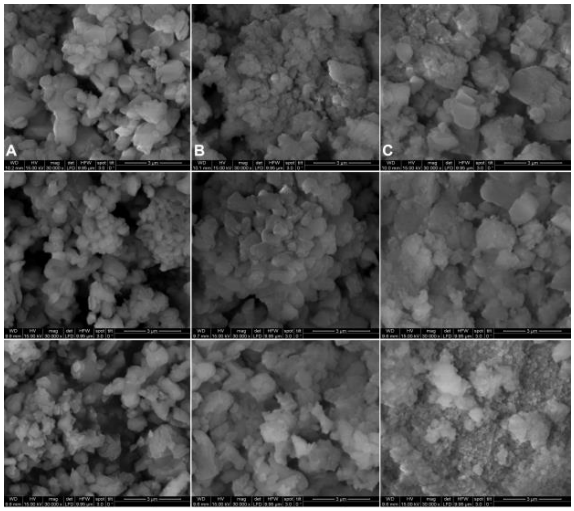

Fig. S3: SEM images of the moisture-dependent CaO carbonatization. In column A the carbonatization in the absence of H_2O, in column B in the presence of 1.25 equivalents and in column C in the presence of 2.5 equivalents is shown. Images are compared for the starting materials (first row), after 30 minutes (second row) and after 120 minutes (third row). Image size 9 x 9 µm

Tab. 1: Cell-parameters of $Sr(OH)_2$, $Sr(OH)_2{\cdot}H_2O$ and $SrCO_3$

	SrO	$Sr(OH)_2$	$Sr(OH)_2$ H_2O	$SrCO_3$
	cubic	ortho-rhombic	ortho-rhombic	ortho-rhombic
Space group	$F\,m\,\bar{3}\,m$	P n a m	P 2_1 a m	P m c n
Nr°	225	62	26	62
a [A]	5.1615(3)	9.8889(5)	6.7131(7)	5.090(2)
b [A]	5.1615(3)	6.1202(6)	6.1981(6)	8.358(2)
c [A]	5.1615(3)	3.9184(4)	3.6478(4)	5.997(4)
α [°]	90	90	90	90
β [°]	90	90	90	90
γ [°]	90	90	90	90
V[A^3]	137.51	237.15	151.78	255.13

Tab. 2: Cell-parameters of BaO, $Ba(OH)_2$, $Ba(OH)_2{\cdot}H_2O$ and $BaCO_3$

	BaO	$Ba(OH)_2$	$Ba(OH)_2$ H_2O	$BaCO_3$
	cubic	mono-clinic	ortho-rhombic	ortho-rhombic
Space group	$F\,m\,\bar{3}\,m$	$P\,1\,2_1/n\,1$	$P\,m\,c\,2_1$	$P\,m\,c\,n$
Nr°	225	14	26	62
a [A]	5.5391	9.3396(2)	3.8947(4)	5.319(9)
b [A]	5.5391	7.8550(2)	6.3657(6)	8.905(8)
c [A]	5.5391	6.7267(2)	6.9523(7)	6.435(9)
α [°]	90	90	90	90
β [°]	90	95.607(2)	90	90
γ [°]	90	90	90	90
V[A^3]	169.95	491.13	172.36	304.85